

Performance of NSM GFRP Retrofitted Postfire RC Slabs Under Monotonic and Cyclic Loadings

Vui Van Cao^{1, 2*}

¹ Faculty of Civil Engineering, Ho Chi Minh City University of Technology (HCMUT), District 10, Ho Chi Minh City, Vietnam.

² Vietnam National University Ho Chi Minh City, Linh Trung Ward, Thu Duc City, Ho Chi Minh City, Vietnam

Received 26 December 2023; Revised 07 May 2024; Accepted 13 May 2024; Published 01 June 2024

Abstract

This study investigated the performance and mechanical properties of NSM GFRP retrofitted postfire RC slabs under monotonic and cyclic loadings. Experiments were conducted for eight RC slabs exposed to different fires. These postfire slabs were retrofitted with NSM GFRP bars, which were then monotonically and cyclically loaded until failure. The results indicated that the control slab failed in flexure, with steel yielding and a main mid-span crack. NSM GFRP retrofitted postfire slabs failed by either crushing of compressive concrete or rupture of GFRP bars. The tested slabs were characterized by bi-linear behavior. NSM GFRP retrofitting improved the yield and ultimate loads of postfire slabs by 47.2% and 116.4% on average, respectively. Fire duration was confirmed to be a main factor that significantly reduced the elastic stiffness of NSM GFRP retrofitted postfire slabs by 60.9% for 60 min of fire. The average plastic-to-elastic stiffness of NSM GFRP retrofitted postfire slabs was 0.132, which was 32 times that of the control slab. The cyclic loading effect caused substantial stiffness degradation of NSM GFRP retrofitted postfire slabs. The average stiffness degradations were 10.6% and 7.2% for original and NSM GFRP retrofitted postfire slabs, respectively. However, the cyclic loading effect caused negligible strength degradation. The combination of increasing fire duration and the cyclic loading effect significantly decreased ductility. Theoretical analyses were carried out to estimate the yield moments of slabs. The analytical equation demonstrated its accuracy in estimating the yield moment capacity of postfire RC slabs without and with NSM GFRP retrofitting.

Keywords: Fire; Reinforced Concrete; Slab; NSM; GFRP; Retrofitting.

1. Introduction

Fire is an extreme load that causes different extents of damage to structures [1] and slabs [2]. Excluding cases of collapse or minor damage, there are two primary options: 1) retrofitting existing structures; or 2) demolishing and replacing them. The latter is typically considered less economical as it involves the cost of demolition, debris removal, and foundation reprocessing. As such, building owners tend to prefer retrofitting as it is a more cost-effective solution.

Fortunately, fiber-reinforced polymer (FRP) with distinct characteristics, e.g., high tensile strength, light weight, application ease, etc., has proven to be an increasingly effective material for retrofitting structures. Numerous studies have demonstrated that FRP retrofitting solutions can outperform traditional methods of steel braces or enlargement. This is because FRP retrofitting does not occupy the living space or interfere with the architecture, while its weight is negligible. The downtime for FRP retrofitting is relatively short, attracting building owners or managers. FRP retrofitting has been investigated by many researchers [3, 4].

* Corresponding author: cvvui@hcmut.edu.vn

<http://dx.doi.org/10.28991/CEJ-2024-010-06-017>



© 2024 by the authors. Licensee C.E.J, Tehran, Iran. This article is an open access article distributed under the terms and conditions of the Creative Commons Attribution (CC-BY) license (<http://creativecommons.org/licenses/by/4.0/>).

The near-surface mounted (NSM) FRP technique has been proven to be more effective than the externally bonded (EB) FRP methods [5–7]. This increased effectiveness is attributed to the fact that NSM FRP is working with inner concrete. This characteristic is also the reason for choosing the NSM technique to retrofit postfire-reinforced concrete (RC) members using FRP bars [8, 9] and FRP laminates [10, 11]. Various aspects of this technique have been reviewed by researchers [12–14].

The NSM FRP retrofit of RC slabs at room temperature has been the subject of several investigations. Sabbaghian & Kheyroddin [15] experimentally and analytically indicated that the strength of one-way RC slabs improved by 92%–326% when retrofitted with high-performance fiber-reinforced cementitious composite laminates with GFRP and steel bars. Silva and Gamage [16] retrofitted RC slabs with a combination of CFRP flexure and shear dowels and found that the punching shear capacity of the retrofitted slabs improved by 120%. Yazdani et al. [17] used CFRP sheets to retrofit prestressed reinforced self-consolidating concrete (SCC) slabs and found that retrofitting with one ply of CFRP improved the flexural capacity by 30% and the absorbed energy by 71%, but decreased the crack width by 23%. Retrofitting with two plies of CFRP slightly further increased the flexural capacity, whereas it prevented the rupture of transverse CFRP. Kamonna & Al-Sada [18] tested seven retrofitted continuous slabs using different configurations of NSM CFRP and steel bars, and they confirmed that the NSM method substantially improved the strength and behavior of the slabs. Zheng et al. [19] retrofitted RC slabs using combinations of CFRP laminates and steel plates and found that this combined retrofitting method increased the ultimate strength and stiffness by 204.2% and 91%, respectively. Kankeri et al. [20] used NSM CFRP and hybrid methods to retrofit pre-cracked hollow core slabs. In the hybrid method, concrete-bonded overlay and NSM CFRP were used to retrofit in the compression and tension zones, respectively. The results indicated that NSM CFRP and hybrid methods improved the ultimate strength by 50% and 130%, respectively.

In fire events, slabs are obviously the most vulnerable component because fire directly affects the bottom surface of slabs. Assessments of fire-exposed RC slabs have been conducted by researchers. Kodur & Bhatt [21] numerically investigated the behavior of FRP-retrofitted concrete slabs in fire and indicated that FRP-retrofitted RC slabs have a lower fire resistance than conventional ones. Bond degradation due to fire significantly affected the fire performance of FRP retrofitted RC slabs, and it should thus be taken into account when predicting fire resistance. Bilotta et al. [22] developed finite element models of FRP RC slabs in fire, considering the material and geometric nonlinearity. The results of parametric analyses showed that the behavior of FRP RC slabs in fire was greatly affected by the boundary conditions. Huang [23] considered concrete spalling in developing a model to study the performance of concrete slabs in fire and found that the membrane effect significantly reduced the concrete spalling impact on the performance of slabs in fire. Lim et al. [24] used SAFIR to model two-way RC slabs in fire and confirmed that these slabs had high fire resistance when membrane action and double curvature deformation appeared. Huang et al. [25] employed their model [26] to analyze the membrane effect in RC slabs in fire, and they indicated that this effect can be properly simulated using nonlinear layer finite elements. Huang et al. [27] later modified the layered element to analyze composite slabs in fire. Lim et al. [28] numerically simulated axial-constraint one-way RC slabs subjected to fire in SAFIR and confirmed the high sensitivity of pin-supported slabs to the axial restraint stiffness and the position of thrust load. Furthermore, the fire resistance of rotation-restrained slabs was higher than that of pin-supported slabs due to moment redistribution. Moss et al. [29] modeled two-way RC slabs in fire and found that the thermal gradient redistributed bending moments and confirmed the benefit of tensile membrane action. Additionally, the sagging moment capacity diminished because the yield steel strength decreased due to fire. Yu & Huang [30] established a layered model with nonlinearity and embedded-weak discontinuity, while Wang et al. [31] proposed concrete constitutive models and a numerical method to predict the behavior of RC slabs exposed to fire. Recently, Azevedo et al. [32] investigated the performance of prestressed NSM-CFRP RC slabs simultaneously under both load and fire and confirmed that the high fire susceptibility of the strengthening system can be solved by the fire protection, which significantly increased the fire resistance to 123–147 min.

In conjunction with modeling, experiments on the performance of fire-exposed RC slabs have been investigated by researchers. Rosa et al. [33] tested GFRP RC slabs under sustained service load and fire, and they indicated that, if regions of GFRP anchorages were controlled between 98–108 °C, the fire resistance of these slabs exceeded 120 min. However, the fire resistance dropped below 20 min if lap splices were exposed to fire. The fire resistance of tested 110-mm-thick slabs increased with the increase in concrete strength but marginally increased when the concrete cover increased from 25 to 35 mm. Wang et al. [34] tested continuous RC slabs in fire and found that the number and the relative position of the heated panels considerably affected the deflections. Meanwhile, the crack modes relied upon the restraints given by adjacent beams and slabs. Wang et al. [35] tested four full-scale RC slabs, which were subjected to both out-of-plane and in-plane loads, under fire. They found that the horizontal restraint force substantially affected the crack modes and induced larger deflections but worse recovery. Wang et al. [36] tested postfire continuous RC slabs exposed to various fires and found that slabs exposed to traveling fire failed by punching-shear or flexural-punching. Additionally, the increase in reinforcement ratio increased the stiffness and ultimate load.

The residual mechanical properties of postfire RC slabs were reduced to some extent; thus, retrofitting of postfire RC slabs is necessary. In this direction, Gao et al. [37] tested nine postfire slabs retrofitted with basalt fabric-reinforced shotcrete, and concluded that the retrofitting increased the flexural capacity by 68.9%–193.4% compared with the

control slabs. The retrofitting also increased the ductility and absorbed energy. Sui et al. [38] tested six postfire hollow RC slabs retrofitted with textile reinforced mortar (TRM) and CFRP and concluded that the retrofitting significantly improved the strength while the increase in CFRP plies reduced the ductility. In the literature, publications on FRP retrofitting of postfire slabs are rarely found.

Retrofitting RC slabs can be divided into the following areas: 1) Retrofitting RC slabs at ambient temperature; 2) Assessments of RC slabs in or after fires; 3) Retrofitting postfire RC slabs. The number of studies on retrofitting RC slabs at ambient temperature seems to be numerous, as reviewed in the fourth paragraph. The extremely complicated nature of fire, the fire safety reasons, and the chemical reaction at elevated temperatures make the second area more difficult than the first area. The combination of this difficulty and the interaction between the added FRP and postfire RC slabs exacerbates the challenge in the third area. This challenge is evidenced by the scarcity of studies on FRP retrofitting of postfire slabs, as reviewed in the seventh paragraph above. Therefore, further studies in the third area should be encouraged. Furthermore, varied loads (loading and unloading), such as live loads, commonly act on slabs. Investigations on various aspects of FRP retrofitted postfire RC slabs under such loadings are necessary, but they are hardly found in the literature. Thus, this current study experimentally and analytically investigated the performance and mechanical properties of NSM GFRP retrofitted postfire RC slabs subjected to monotonic and cyclic loadings. To achieve this goal, experiments were conducted on eight RC slabs. These eight RC slabs were exposed to 0 (control), 20, 40, and 60 min of ISO 834 fires. These postfire slabs were retrofitted with NSM GFRP bars. The NSM GFRP retrofitted postfire slabs were monotonically and cyclically loaded. The failure mode, behavior, cyclic loading effect, and mechanical properties of NSM GFRP retrofitted postfire slabs were analyzed. Finally, NSM GFRP retrofitted postfire slabs were theoretically analyzed to estimate the yield moment capacity of the tested slabs. The technical information of experimental and theoretical results can be helpful for structural engineers in the field of FRP retrofitting design of postfire slabs.

2. Experimental Program

2.1. Concrete, Steel, GFRP, and Resin

Table 1 shows the concrete mix used to cast the slabs. Figure 1 presents the grading curves of sand and stone aggregates, in which the upper and lower bounces [39] were also plotted. Six cubic concrete samples 150×150×150 mm were prepared and tested (Figure 2-a). The average strength of the cubic samples at 28 days was 31.2 MPa. The equivalent standard cylinder compressive strength approximated $31.2/1.2 = 26.0$ MPa. Thread surface GFRP bars with an outer diameter of 6 mm were used for NSM GFRP retrofitting. The real diameter, the nominal ultimate tensile strength, and the nominal elastic modulus these GFRP bars were 5.15 mm, 800 MPa, and 45000 MPa, respectively, as provided by the manufacturer. The reinforcement was steel $\phi 8$, and five samples of steel were tested (Figure 2-b). Their average yield and ultimate tensile strengths were 353.7 MPa and 424.3 MPa, respectively.

Table 1. Concrete mix

Material	Volume per m ³
PCB40 cement	339 kg
Coarse aggregate, stone 10–20 mm	1201 kg
Sand ≤ 2.5 mm	684 kg
Water	190 liters

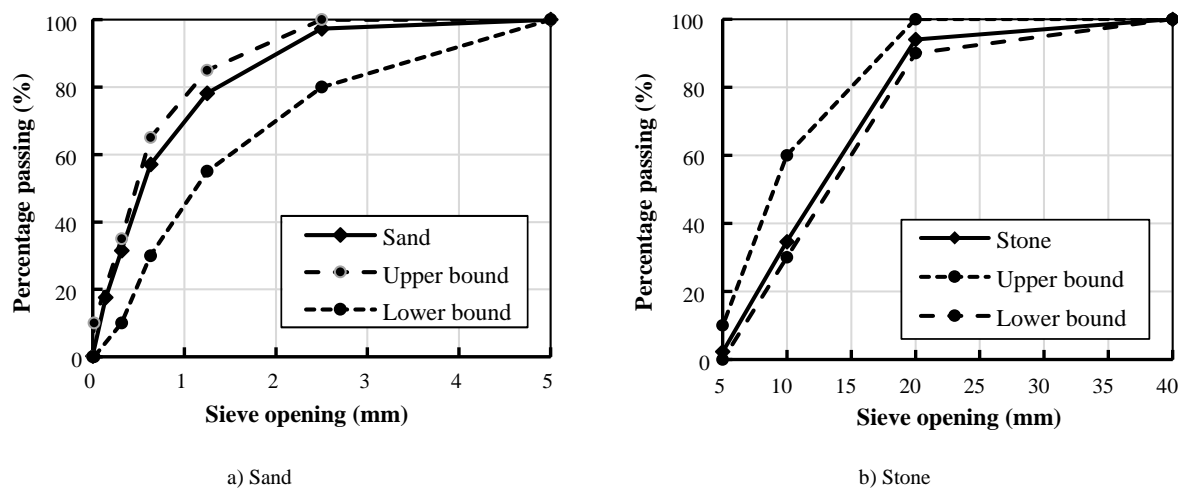


Figure 1. Grading curves of sand and stone aggregates



Figure 2. Specimens after testing

2.2. Slabs and Fabrication

Eight RC slabs (1600 × 400 × 80 mm) were used for the tests. Figure 3 shows the configuration of the tested slabs. Steel $\phi 8$ was used for both longitudinal and transverse reinforcement. The longitudinal reinforcement was designed in accordance with ACI 318-19 [40]. A clear concrete cover of longitudinal steel was 15 mm, as previously used by researchers [16, 18, 37]. Figure 4 shows eight slabs before the fire tests. Table 2 presents the names, fire durations, and NSM GFRP strengthening of the slabs. Eight slabs were categorized into two groups, namely R0 and R1, which were subjected to monotonic and cyclic loading, respectively. In each group, four slabs were exposed to 0, 20, 40, and 60 min, which were named F0, F1, F2, and F3, respectively. The letter F represents fire, while the numbers 0, 1, 2, and 3 represent the fire durations divided by 20. Figure 5 presents the flowchart of the experiments.

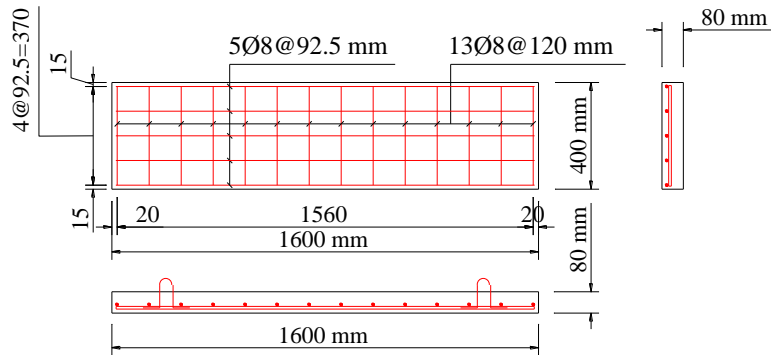


Figure 3. Steel reinforcement of slabs



Figure 4. RC slabs before fire tests

Table 2. Names, fire duration, and FRP retrofitting of slabs

No.	Group	Slab	Fire	Condition	FRP retrofitting	Loading	Note
1		F0-R0	0	no fire	No	Monotonic	Control slab
2	R0	F1-R0	20	Fire-exposed	NSM GFRP	Monotonic	
3		F2-R0	40	Fire-exposed	NSM GFRP	Monotonic	
4		F3-R0	60	Fire-exposed	NSM GFRP	Monotonic	
5		F0-R1	0	no fire	NSM GFRP	Cyclic	
6	R1	F1-R1	20	Fire-exposed	NSM GFRP	Cyclic	
7		F2-R1	40	Fire-exposed	NSM GFRP	Cyclic	
8		F3-R1	60	Fire-exposed	NSM GFRP	Cyclic	

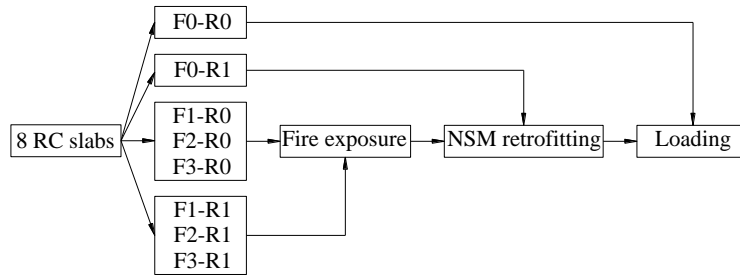


Figure 5. Flowchart of experiments

2.3. Fire Test Setup

The fire tests were performed in a furnace. The furnace consists of a steel frame structure, high temperature resistant brick layers, an oil burner, a thermocouple system, two cover blocks, and an exhaustive pipe. The thermal system capacity was 1200°C. The volume of oil for burning can be adjusted to control the temperature in the furnace. Figure 6-a shows a slab installed in the furnace, and Figure 6-b shows the installation of a ceramic cotton layer on the top of the slab for temperature isolation on the top surface. After the installation of the ceramic cotton layer, two cover blocks were placed on top to cover the furnace, which helped to prevent energy loss and control the temperature easily. Due to fire safety reasons, the fire tests were conducted at nights. Each fire test was conducted each night. Figure 7 shows the obtained temperature–time curves of the tested slabs. Figure 7 also shows the ISO 834 temperature–time curve for comparison. Due to the control of the oil input, the obtained temperature–time curves were very close to the ISO 834 temperature–time curve. At the designed fire durations, the oil burner was turned off, and the temperature decreased significantly with time. These descending branches of temperature–time curves are also plotted in Figure 7.

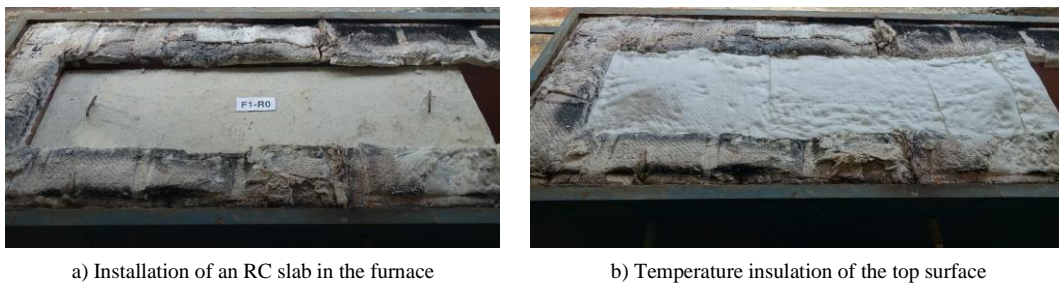


Figure 6. Fire test setup

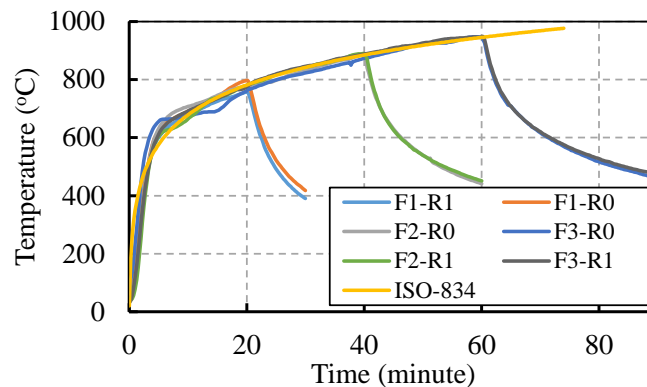


Figure 7. Temperature–time curves

After the fire test of each slab, the slab was left in the furnace until the next day to cool down to the normal temperature. Two cover blocks were lifted and moved out. Then, the slab was lifted up and moved out of the furnace. When the postfire slabs were lifted, pictures were taken from the bottom of the slabs. Figure 8 shows examples of the bottom surfaces of slabs before and after fire exposure. Minor concrete spalling and hair cracks appeared on the bottom surfaces of postfire slabs.

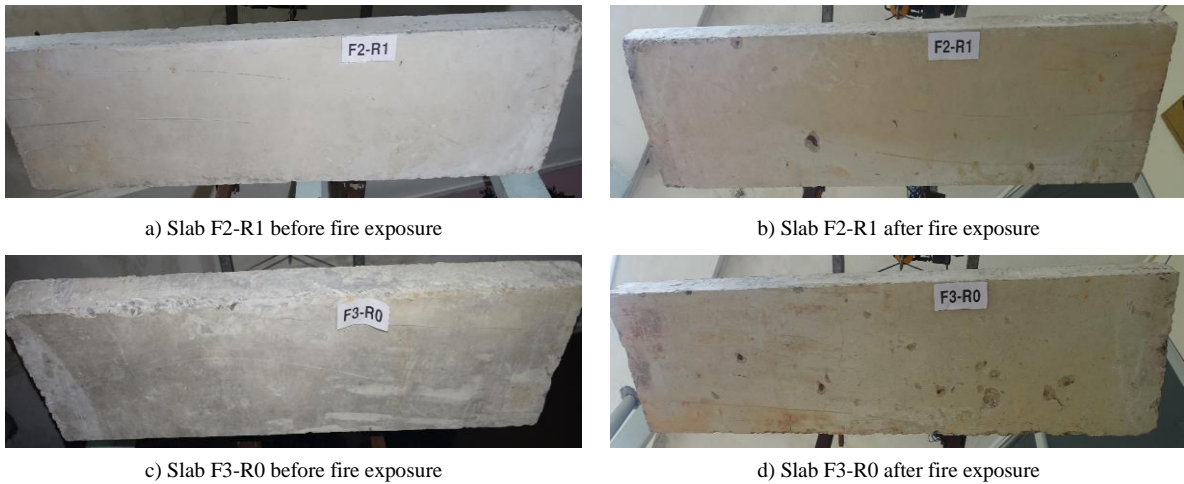


Figure 8. Examples of bottom surfaces before and after fire exposure

2.4. NSM GFRP Retrofitting

NSM GFRP technique was implemented to retrofit the slabs. The postfire slabs were grooved using a grooving machine. The dimensions of the grooves were 10 × 10 mm, which were selected based on: 1) 1.5 times the diameter of GFRP bars, as recommended by ACI [41] and Singh et al. [42]; 2) the concrete cover thickness of 15 mm; and 3) some recommendations by Kalayci et al. [43], Soliman et al. [44], and Sharaky et al. [45]. After grooving, the bottoms of the grooves were ground using a grinding machine. Finally, a vacuum cleaner was used to remove dust in grooves and on the slab surfaces. The length of the NSM GFRP bars was 1400 mm. There were five NSM GFRP bars for each slab. The distance between the grooves was 93 mm. Figure 9 shows the design of NSM GFRP retrofitting.

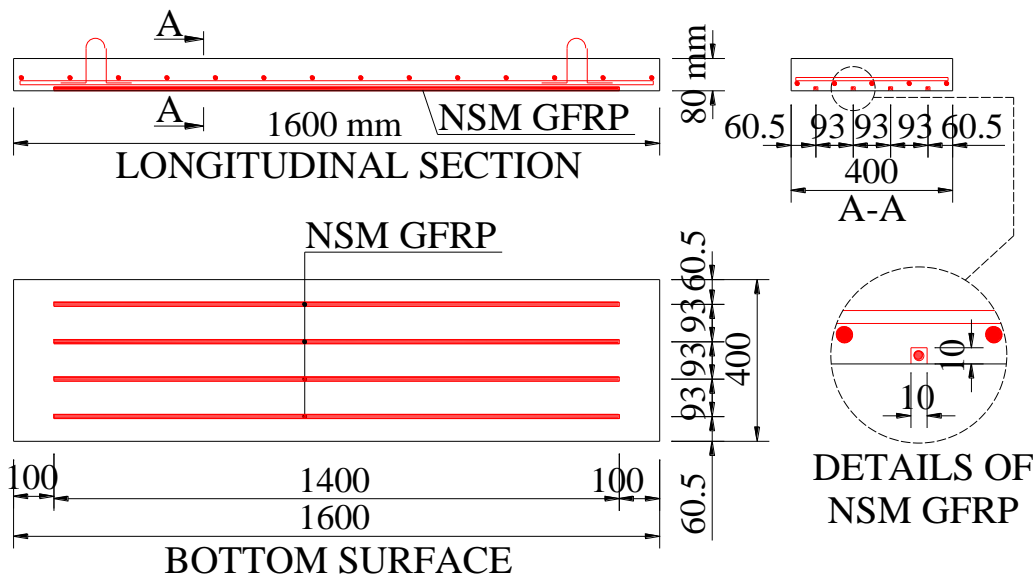


Figure 9. NSM GFRP retrofitting of postfire slabs

After the fire tests, NSM GFRP retrofitting was performed on the postfire slabs. The post-fire slabs were turned upside down. Because the slabs were singly reinforced by steel located on the tension side, the tensile and compression sides should be unchanged when they were turned upside-down to avoid failure. Therefore, they were supported in the middle by sand bags, which can be seen in Figure 10. A grooving machine was used to cut grooves. Then, the bottom surfaces of the grooves were ground using a grinding machine. A vacuum cleaner was used to remove dust in the

grooves. Figures 10-a and 10-b show the slabs after grooving and retrofitting, respectively. Figure 10-c shows a close view of the grooves before retrofitting. Two-component resin was mixed with a regulated ratio and added into the grooves to about 1/3 the groove depth. Then, FRP bars were placed into the grooves. Finally, the resin was added to fill the grooves. Figure 10d shows a close view of slabs after retrofitting.

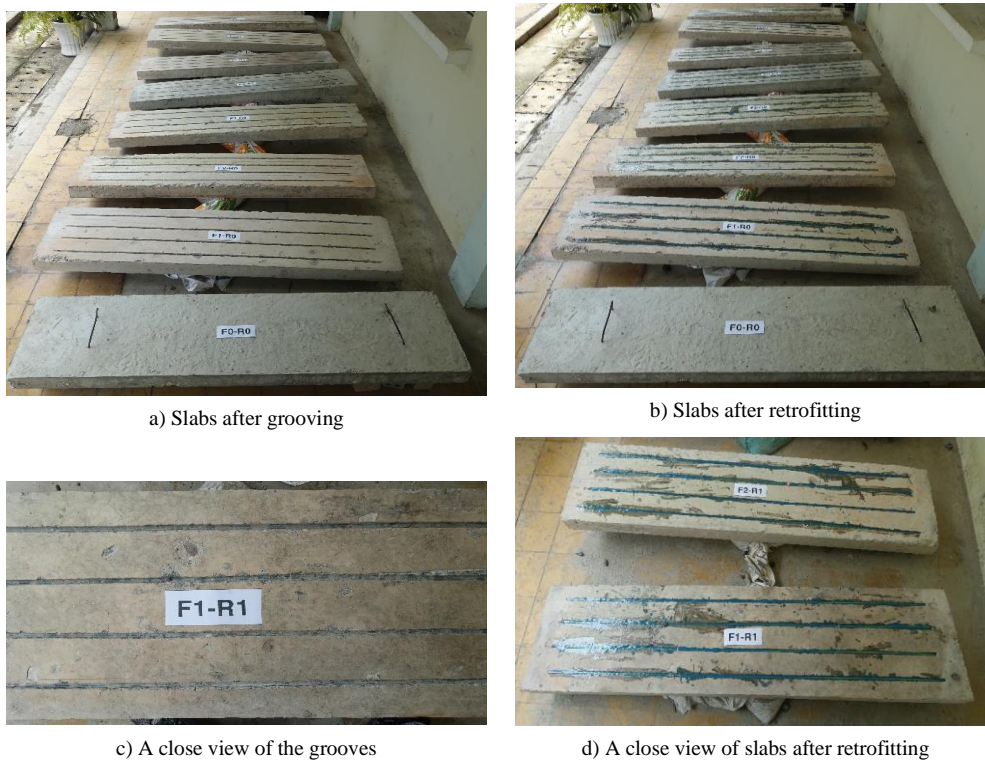


Figure 10. NSM GFRP retrofitting of postfire slabs

2.5. Monotonic and Cyclic Loadings

The cyclic loading was based on the displacement control. For monotonic loading, the deflection was compulsorily increased until the slabs failed. For the cyclic loading, the deflection was gradually increased to the peak deflection of the first cycle and then gradually released until the load was close to zero. Then, the slabs were loaded to the peak deflection of the next cycle, and so on. It can be noted that the deflection at the zero load of each cycle was the residual deflection of the slabs. The peak deflection of the i^{th} cycle was $\Delta = i \times \Delta_0$, in which Δ_0 is selected to be $0.5\Delta_y$ and Δ_y is the yield deflection of the control slab under monotonic loading. Figure 11 illustrates the cyclic loading applied to the tested slabs. To determine the peak deflection for the cyclic loading, the control slab under monotonic loading was tested first, and its result is presented in Section 3.2. For convenience, the yield deflection of the control slab is mentioned herein as $\Delta_y = 8.00$ mm. Therefore, the peak deflections of cycles 1, 2, 3, ... were 4 mm, 8 mm, 12 mm, ..., respectively.

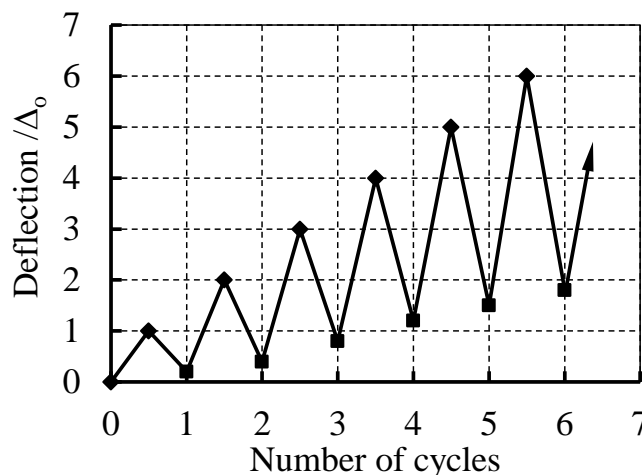


Figure 11. Cyclic loading

2.6. Loading Test Setup

Figures 12-a and 12-b show the side and angle views of the experiment setup. A load cell was bolted to the movable end of the hydraulic jack to measure the load, which can be seen in Figures 12-a and 12-b. Three linear variable displacement transducers (LVDT) were used. One was located at the mid-span bottom of the slabs to measure the deflections during loading (Figure 12-c), while the other two were located at the two supports to measure the support settlement (if any). Figure 12-d shows the diagram of the slabs under loading. The support distance or span length was 1500 mm. Prior to the main tests, the slabs were loaded to 500 N and released to zero load to eliminate contact errors. The slabs were then loaded as designed until they failed. During loading tests, the loads and deflections were simultaneously recorded. The tests were terminated when the slabs failed. The failure was indicated by the drop in load, the rupture of GFRP bars, or the large cracks in slabs.

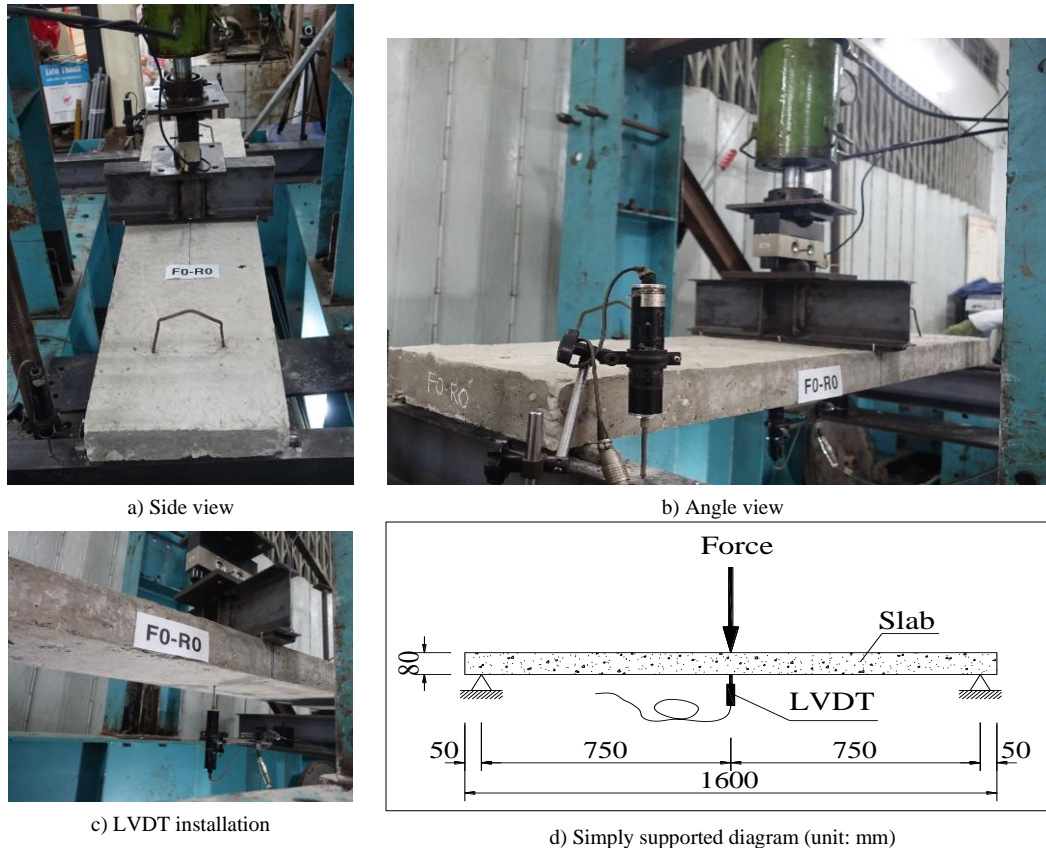


Figure 12. Experiment setup

3. Experimental Results and Discussion

3.1. Failure Modes

Figure 13 shows the failure modes of the tested slabs. Slab F0-R0 failed in flexure, as shown in Figure 13-a, in which a large crack appeared at the mid-span. No crushing of concrete on the top surface was observed on slab F0-R0. The large mid-span crack resulted from the yielding of steel at the largest bending moment. Figure 13-b shows the failure mode of slab F1-R0, which failed by crushing compressive concrete. The crushing of concrete was followed by the shear failure of concrete, while no rupture of NSM GFRP was observed. The failure mode of slab F2-R0 was almost similar to that of slab F1-R0, but the crushing of concrete was less severe and the shear failure was not clearly developed (Figure 13-b). Rupture of NSM GFRP bars occurred in some slabs, whereas debonding and peeling-off of NSM GFRP bars were not observed in any slabs.

A major difference between the NSM GFRP retrofitted postfire slabs (Figures 13-b to 13-h) and the control slab (Figure 13-a) is the development and distribution of cracks. For the control slab, there was one large crack at the mid-span, while fewer cracks occurred in the adjacent regions of the mid-span. For the NSM GFRP retrofitted postfire slabs, the presence of NSM GFRP prevented the large mid-span crack and distributed the cracks on a larger mid-span region of the retrofitted slabs. This distribution can be explained by the fact that, after yielding of steel, the tensile stress in NSM GFRP bars continued to increase linearly while the stress in steel bars remained constant. The tensile strain in concrete was governed by not only the stress in steel but also the stress in NSM GFRP. The linearity of GFRP plays an important role in distributing the tensile strain and, in turn, the cracks. Another different point is that, after failure and after releasing the load to move the slabs out of the testing position, NSM GFRP retrofitted postfire slabs recovered to an almost straight state, while the control slab exhibited a minor recovery.

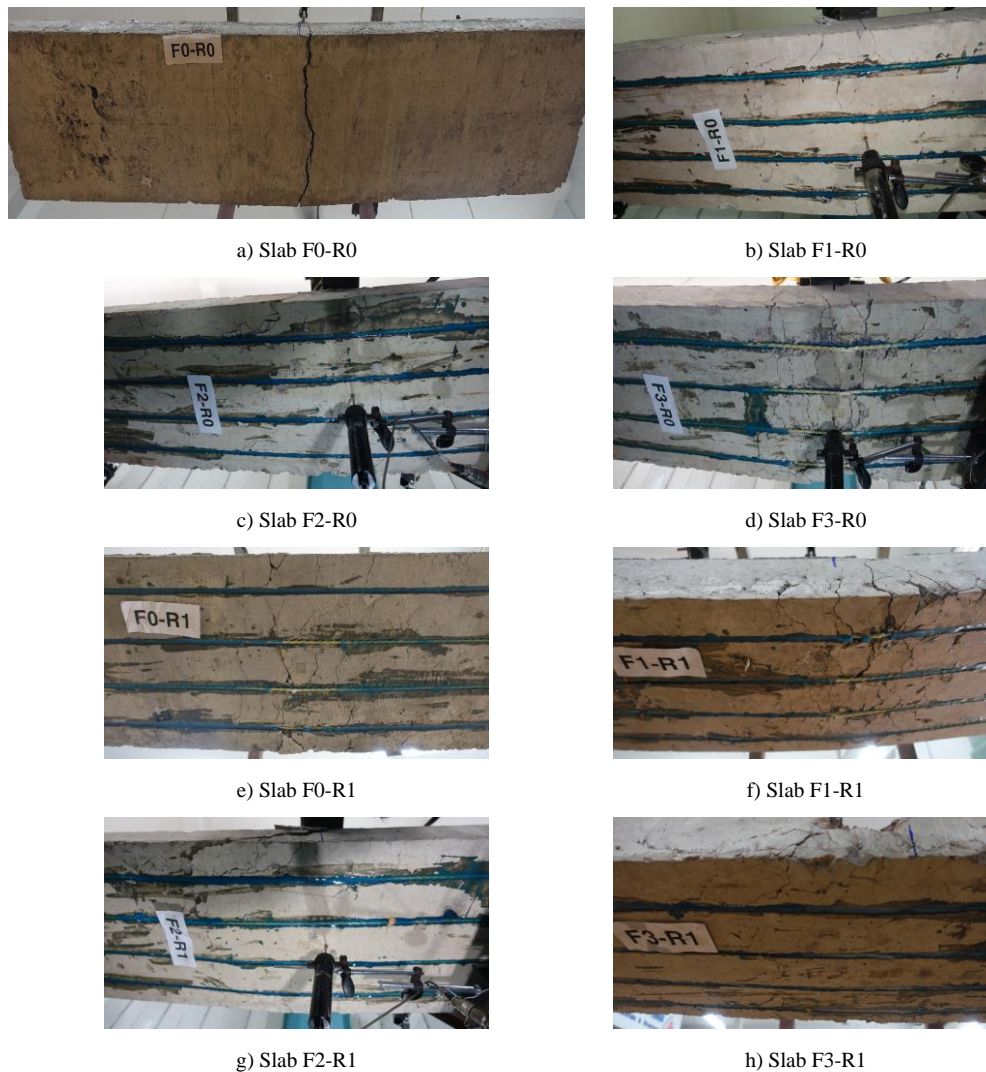


Figure 13. Failure modes

3.2. Load–deflection Behavior

Figures 14-a to 14-h plot the load–deflection curves of the tested slabs on the same axis limit coordinate system for visual comparison. The envelope curves of slabs under cyclic loading were plotted in red curves (Figures 14-e to 14-h). Figures 14-a to 14-h also show the yield point, ultimate point, and their coordinates. The yield points divided the curves into the pre-yield and post-yield branches. These branches can be idealized by straight lines, which are plotted by the dashed lines in Figures 14-a to 14-h. It is noted that the idealized curves of cyclically loaded slabs were determined based on the envelope curves.

NSM GFRP retrofitted postfire slabs (Figures 14-b to 14-h) exhibited significantly higher yield and ultimate strengths compared with the control slab (Figure 14-a). The retrofitted postfire slabs also had higher yield and ultimate deflections. These increments can be explained by the contribution of NSM GFRP bars to the tension force on the cross section. GFRP bars shared the tension force with steel bars; therefore, a higher tension force was required to reach the yielding state of steel. Consequently, the yield load and the yield deflection increased. After yielding, the resistance force of steel was constant due to its yielding, while the resistance force of NSM GFRP bars linearly increased. This linear increase in the resistance of NSM GFRP bars was the reason for the increase in the ultimate load.

Overall, the load–deflection behavior of the GFRP retrofitted postfire slabs can be classified into three phases: pre-yield, post-yield, and failure. The yield point distinguished the elastic and plastic phases. The mechanism of these phases of the control slab was quite clear because it totally depended on the steel yielding. For the GFRP retrofitted postfire slabs, the pre-yielding mechanism is slightly different. This difference is because the contribution of NSM GFRP to the tension force was still marginal, while the tension force was governed by steel. In contrast, the post-yielding mechanism of NSM GFRP retrofitted postfire slabs was completely different from the control slab. This difference is explained by the fact that, in the post-yielding state, the tension force in slabs was governed by the NSM GFRP, while the tension force of steel bars remained constant.

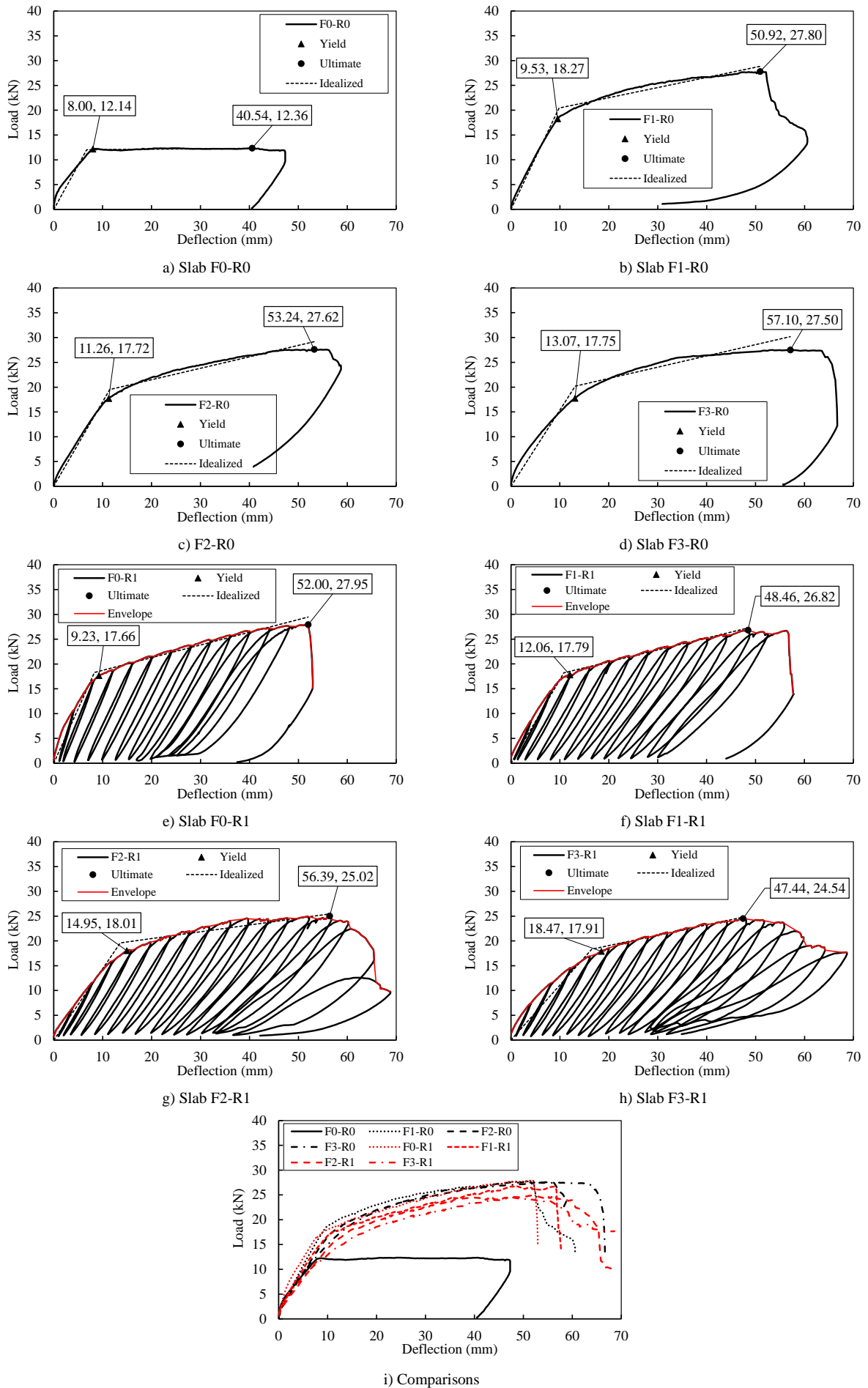


Figure 14. Load-deflection curves of slabs

For general comparisons, all load–deflection curves (Figures 14-a to 14-h) were plotted in Figure 14-i. In this figure, the black and red curves are of monotonically and cyclically loaded slabs, respectively. For the cyclically loaded slabs, their envelope curves, instead of the cyclic curves, were plotted to avoid visual difficulty. Although postfire slabs were negatively affected by fire exposure, compared with the control slab F0-R0, Figure 14i indicates the following aspects:

- The NSM GFRP retrofitted postfire slabs exhibited a substantial improvement in their behavior;
- NSM GFRP retrofitting substantially improved the yield and ultimate load-carrying capacities;
- NSM GFRP retrofitting increased both elastic and plastic stiffness. Except for the long fire duration of 60 min, the elastic stiffness of other slabs is higher than that of the control slab.
- NSM GFRP retrofitting increased the yield and ultimate deflections.
- The load–deflection curves of cyclically loaded slabs (the red curves) are lower than those of monotonically loaded slabs (the black curves), indicating the negative effect of the cyclic loading.

The above general comparisons indicate the effectiveness of NSM GFRP retrofitting. Details of the comparisons are presented in the following sections.

3.3. Yield Load

Figure 15-a presents the yield loads of the tested slabs. Slab F0-R0 has a yield load of 12.1 kN, while those of slabs F1-R0, F2-R0, and F3-R0 are 18.3 kN, 17.7 kN, and 17.8 kN, respectively. Compared with the control slab F0-R0, the yield loads of slabs F1-R0, F2-R0, and F3-R0 increased by 50.5%, 46.0%, and 46.2%, respectively, as compared in Figure 15-b. The yield load of slab F0-R1 was 17.7 kN, which is 45.5% higher than that of the control slab. The yield loads of slabs F1-R1, F2-R1, and F3-R1 increased to 18.0 kN, 17.9 kN, and 17.9 kN, increasing 46.5%, 48.4%, and 47.5%, respectively, compared with the yield load of the control slab. Overall, the yield loads of postfire slabs are substantially close to one another. On average, NSM GFRP retrofitting increased the yield load by 47.2%, indicating the negligible effect of fires on the yield load. This can be explained by the fact that the fire exposed to the bottom slab surface and thus has negligible impact on the top slab surface, where the concrete resists the compression force. Additionally, the impacts of fire on the bottom surface reduce the strengths of steel and concrete near the bottom surface. The reduction in steel strength can be recoverable when the temperature goes down to room temperature [29], whereas the reduction in concrete strength is irrecoverable. The reduction of concrete strength around the steel bars might have a negligible impact on the bond between the steel bars and concrete and thus negligibly affect the yield load.

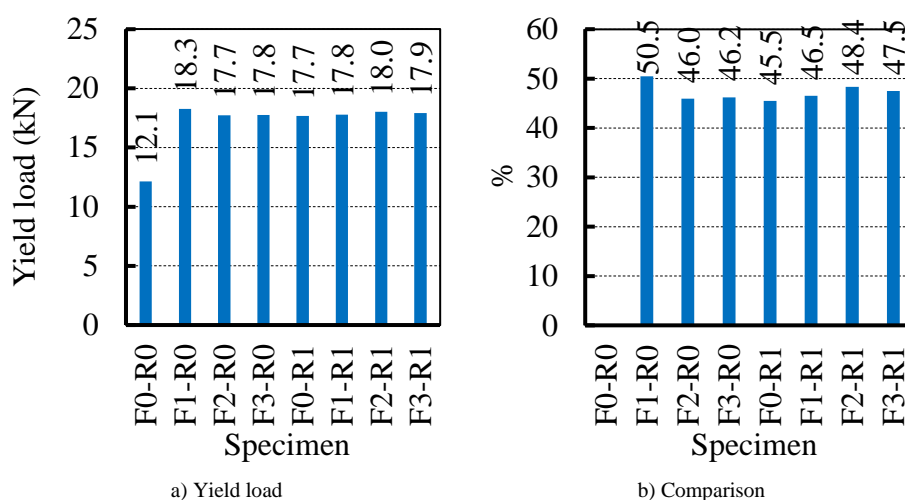


Figure 15. Yield load

3.4. Yield Deflection

Figure 16-a presents the yield deflections of slabs. Under monotonic loading, the yield deflection of slab F0-R0 was 8.0 mm, while yield loads of NSM GFRP retrofitted postfire slabs F1-R0, F2-R0, and F3-R0 increased to 9.5 mm, 11.3 mm, and 13.1 mm, respectively. Compared with the yield deflections of slab F0-R0, the yield deflections of NSM GFRP retrofitted postfire slabs F1-R0, F2-R0, and F3-R0 increased by 19.1%, 40.8%, and 63.4%, respectively, as compared in Figure 16-b. Therefore, the increase in yield deflection of these slabs is due to the fire effect.

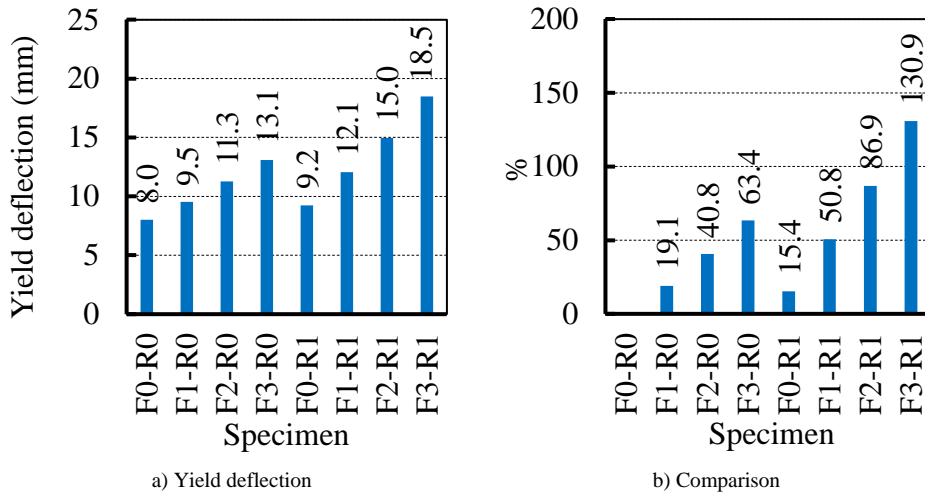


Figure 16. Yield deflection

Under cyclic loading, the NSM GFRP retrofitted slab F0-R1 had a yield deflection of 9.2 mm, which is 15.4% higher than that of slab F0-R0. This indicates that the NSM GFRP retrofitting slightly increased the yield deflection of the slab. The yield deflections of slabs F1-R1, F2-R1, and F3-R1 increased to 12.1 mm, 15.0 mm, and 18.5 mm, which are 50.8%, 86.9%, and 130.9% higher than that of the control slab. These increments also confirm the effects of fire on increasing the yield deflection of the postfire slabs. The yield deflection increases with the increase in fire duration.

3.5. Ultimate Load

Figure 17-a presents the ultimate loads of the tested slabs. Under monotonic loading, the ultimate load of the control slab F0-R0 was 12.4 kN, while the ultimate loads of NSM GFRP retrofitted postfire slabs F1-R0, F2-R0, and F3-R0 were 27.8 kN, 27.6 kN, and 27.5 kN, respectively. Compared with the control slab, the ultimate loads of slabs F1-R0, F2-R0, and F3-R0 significantly increased by 124.9%, 123.5%, and 122.5%, respectively, as compared in Figure 17-b. These increments indicated that, despite the reduction in the ultimate load due to fires, NSM GFRP retrofitting is an effective solution for increasing the ultimate load.

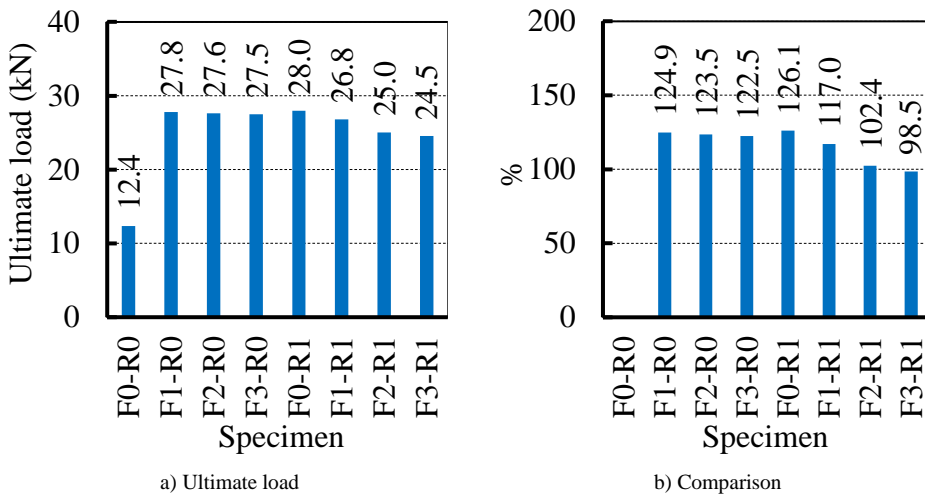


Figure 17. Ultimate load

Under cyclic loading, the ultimate load of slab F0-R1 was 28.0 kN, while the ultimate loads of retrofitted postfire slabs F1-R1, F2-R1, and F3-R1 were 26.8 kN, 25.0 kN, and 24.5 kN, respectively. Compared with the control slab, the ultimate loads of slabs F1-R1, F2-R1, and F3-R1 significantly increased by 117.0%, 102.4%, and 98.5%, respectively. These increments are lower than those of the monotonic loading slabs, indicating that the cyclic loading effect decreased the ultimate loads. NSM GFRP retrofitting exhibits its effectiveness in improving the ultimate load by 116.4% on average.

3.6. Ultimate Deflection

Figure 18-a presents the ultimate deflections of the tested slabs. The ultimate deflection of the control slab was the lowest at 40.5 mm. Under monotonic loading, the yield deflections of slabs F1-R0, F2-R0, and F3-R0 were 50.9 mm,

53.2 mm, and 57.1 mm, respectively. Compared with the control slab, the ultimate deflections of slabs F1-R0, F2-R0, and F3-R0 increased by 25.6%, 31.3%, and 40.8%, respectively, as compared in Figure 18-b. The ultimate deflection increased with the increase in fire duration.

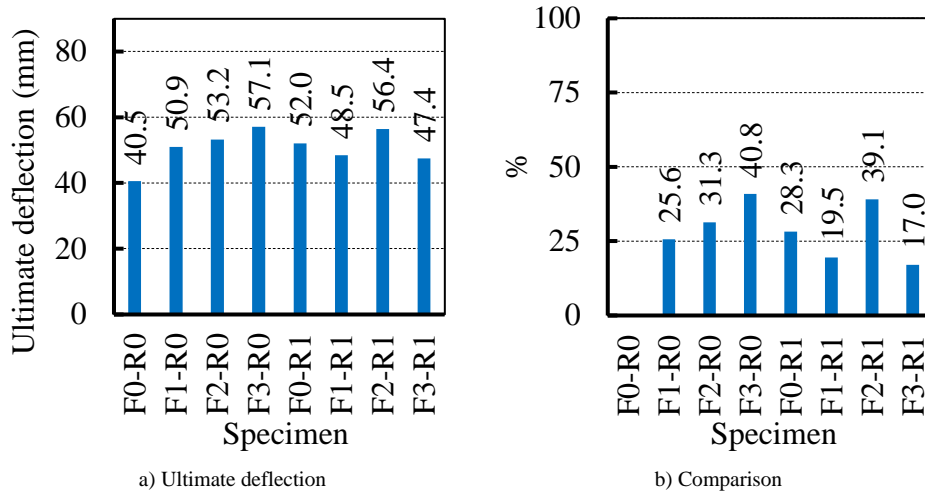


Figure 18. Ultimate deflection

Under cyclic loading, the ultimate deflection of retrofitted slab F0-R1 was 52.0 mm, increasing by 28.3% compared with that of the control slab. The ultimate deflections of retrofitted postfire slabs F1-R1, F2-R1, and F3-R1 were 48.5 mm, 56.4 mm, and 47.4 mm, which increased by 19.5%, 39.1%, and 17.0% compared with the ultimate deflection of the control slab, respectively. There is no clear trend in the cyclic loading effects on the ultimate deflection, probably due to the cumulative damage caused by the cyclic loading.

3.7. Elastic Stiffness

Figure 19-a presents the elastic stiffness of the tested slabs, which is the slope of the idealized line of the zero-to-yield branch. The elastic stiffness of control slab F0-R0 was 1.79 kN/mm. The elastic stiffness of the retrofitted postfire slab F1-R0 was 2.08 kN/mm. When the fire duration increased to 40 min and 60 min, the elastic stiffness of slabs F2-R0 and F3-R0 decreased to 1.71 kN/mm and 1.54 kN/mm, respectively. Compared with the control slab, the elastic stiffness of slab F1-R0 increased by 16.2%, and that of slabs F2-R0 and F3-R0 decreased by 4.5% and 14.0%, respectively, as compared in Figure 19-b. This indicates that the increase in fire duration significantly decreased the elastic stiffness.

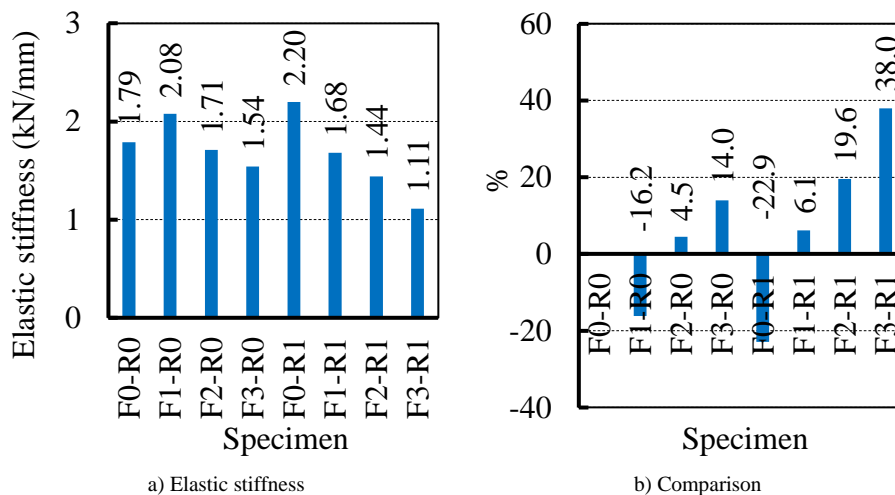


Figure 19. Elastic stiffness

Under cyclic loading, the yield stiffness of slab F0-R1 was 2.20 kN/mm, which is the highest elastic stiffness among the tested slabs. This highest elastic stiffness is a result of two conditions: 1) this slab was not exposed to fire, and 2) the presence of NSM GFRP. Due to the effects of 20, 40, and 60-min fires, the elastic stiffnesses of NSM GFRP retrofitted slabs F1-R1, F2-R1, and F3-R1 were 1.68, 1.44, and 1.11 kN/mm, respectively. Compared with the elastic stiffness of the control slab, that of slab F0-R1 increased by 22.9%, while that of slabs F1-R1, F2-R1, and F3-R1 increased by 6.1%,

19.6%, and 38.0%, respectively. Compared with the elastic stiffness of slab F0-R1, the elastic stiffness of slabs F1-R1, F2-R1, and F3-R1 increased by 29.0%, 42.5%, and 60.9%, respectively. These results reveal the substantial effect of fire duration on elastic stiffness.

3.8. Plastic Stiffness

The plastic stiffness (the slope of the plastic branch) was determined using the Excel procedure, as mentioned above. Figure 20-a shows the plastic stiffness, while Figure 20-b presents the comparisons of the plastic stiffness of NSM GFRP retrofitted slabs against that of the control slab. The control slab F0-R0 had a plastic stiffness of 0.008 kN/mm. NSM GFRP retrofitting increased the plastic stiffnesses of slabs F1-R0, F2-R0, and F3-R0 to 0.205, 0.231, and 0.227 kN/mm, which are 24.6, 27.9, and 27.4 times the plastic stiffness of the control slab, respectively.

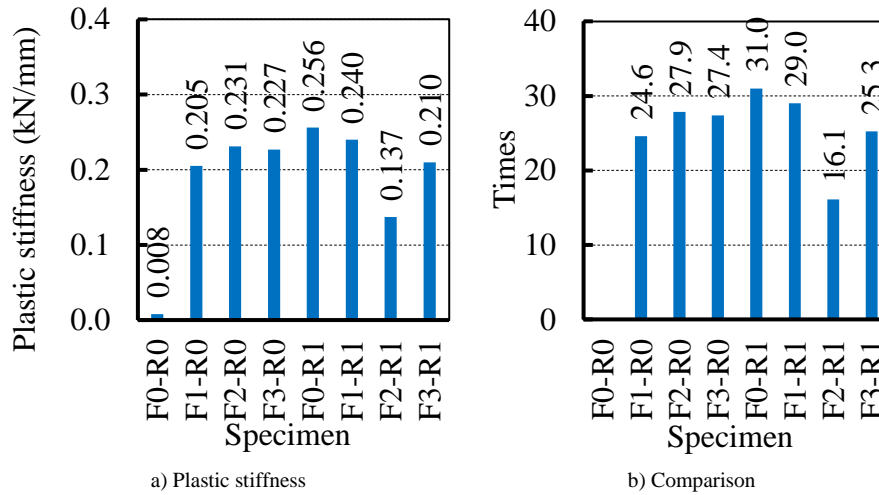


Figure 20. Plastic stiffness

Under cyclic loading, slabs F0-R1 had a plastic stiffness of 0.256 kN/mm, which is slightly higher than that of the retrofitted slabs under cyclic loading. NSM GFRP retrofitted postfire slabs F1-R1, F2-R1, and F3-R1 had plastic stiffnesses of 0.240, 0.137, and 0.210 kN/mm, which are 29.0, 16.1, and 25.3 times that of the control slab, respectively. The plastic stiffness of group R1 slabs exhibited a larger variation and was lower than that of group R0 slabs, indicating the negative effect of cyclic loading on the plastic stiffness. This is because the cyclic loading caused opening and closing cracks, which could possibly cause degradation of concrete strength. Additionally, the cyclic loading also caused the degradation of the bond between reinforcement (steel and GFRP) and concrete.

3.9. Ratios of Plastic Stiffness to Elastic Stiffness

Table 3 presents the ratios of plastic stiffness (taken from Section 3.8) to elastic stiffness (taken from Section 3.7) of the tested slabs. The control slab had a ratio of 0.004, while the NSM GFRP retrofitted postfire slabs had ratios varying from 0.095 to 0.189, making the average ratio of 0.132. Therefore, the average ratio of NSM GFRP retrofitted postfire slabs was 32 times that of the ratio 0.004 of the control slab. This is due to the fact that, after yielding of steel, the NSM GFRP still worked within its elastic range. In other words, the plastic stiffness was significantly affected by the NSM GFRP.

Table 3. Ratios of plastic stiffness to elastic stiffness

Group	Slab	Elastic stiffness	Plastic stiffness	Plastic-to-elastic	Average
		(kN/mm)	(kN/mm)	Stiffness ratio	
-1	-2	-3	-4	(5) = (4)/(3)	-6
F0-R0	F0-R0	1.79	0.008	0.004	0.004
F1-R0	F1-R0	2.08	0.205	0.099	
F2-R0	F2-R0	1.71	0.231	0.135	
F3-R0	F3-R0	1.54	0.227	0.147	
F0-R1	F0-R1	2.2	0.256	0.116	0.132
F1-R1	F1-R1	1.68	0.24	0.143	
F2-R1	F2-R1	1.44	0.137	0.095	
F3-R1	F3-R1	1.11	0.21	0.189	

3.10. Ductility

Ductility is calculated by Equation 1, in which Δ_u and Δ_y are the ultimate and yield deflections, respectively.

$$\mu = \frac{\Delta_u}{\Delta_y} \tag{1}$$

Figure 21-a presents the ductility of the tested slabs. The control slab had a ductility of 5.1 (highly ductile), while the NSM GFRP retrofitted postfire slabs F1-R0, F2-R0, and F3-R0 under monotonic loading had ductility of 5.3, 4.7, and 4.4, respectively, classified as highly ductile according to ASCE/SEI 41 [46]. Compared with the ductility of the control slab, the ductility of NSM GFRP retrofitted postfire slabs F1-R0 increased by 3.9% (Figure 21-b), while the ductility of slabs F2-R0 and F3-R0 decreased by 7.8% and 13.7%, respectively. Therefore, the fire duration clearly increased the ductility of these slabs. On average, the ductility of these three NSM GFRP retrofitted postfire slabs was 4.8, which increased by 5.9% compared with that of the control slab.

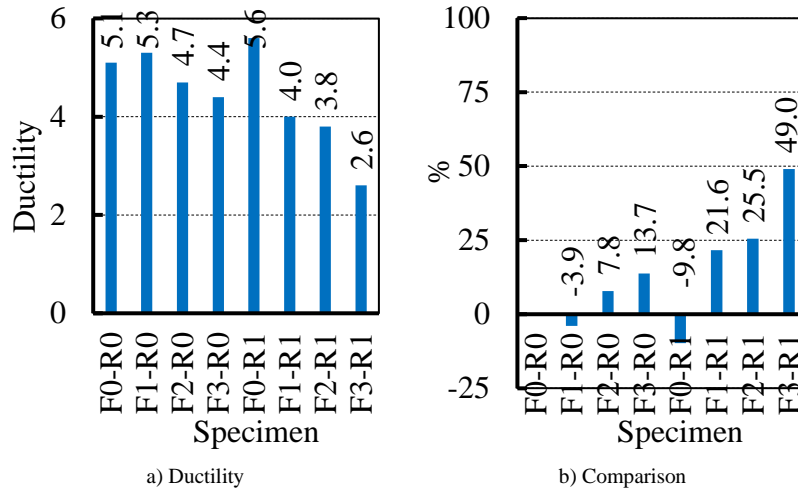
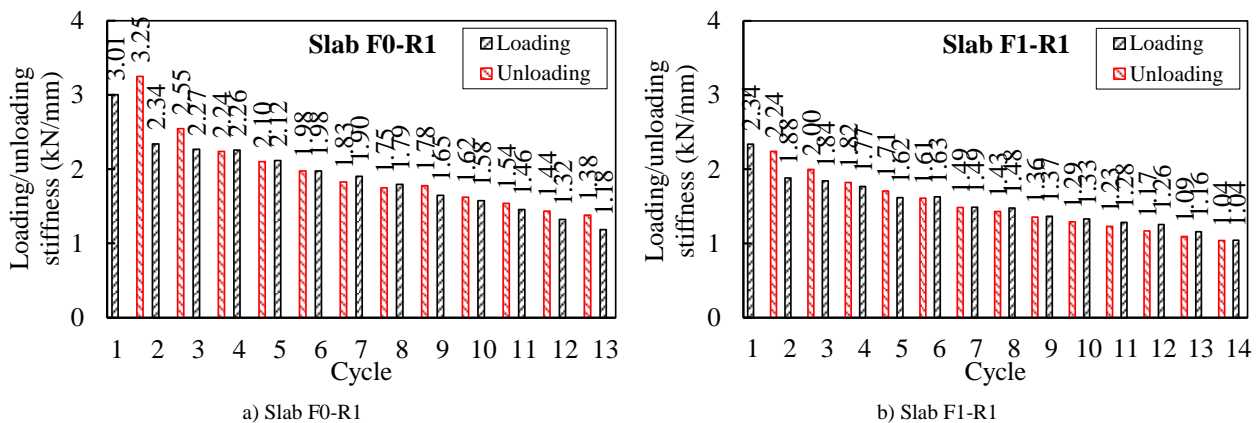


Figure 21. Ductility

For slabs under cyclic loading, the NSM GFRP retrofitted postfire slab F0-R1 had a ductility of 5.6, which was then reduced to 4.0, 3.8, and 2.6 for slabs F1-R1, F2-R1, and F3-R1, respectively. These ductility values classify the slabs as moderately ductile. These results reveal that the combination of fire and cyclic loading clearly decreased the ductility of NSM GFRP retrofitted postfire slabs. This can be explained by the fact that fire previously decreased the bond between the reinforcement (steel and NSM GFRP) bars and postfire concrete; then, the cyclic loading effect additionally decreased this bond, resulting in a substantial decrease in the ductility.

3.11. Loading and Unloading Stiffness

Figure 22 shows the variations in loading and unloading stiffness of NSM GFRP retrofitted postfire slabs under cyclic loading. The black increasing hatch bars are the stiffness of loading, while the red decreasing hatched bars represent the unloading stiffness. The degradations of stiffness were 10.6, 8.4, 6.6, and 6.5%/cycle for slabs F0-R1, F1-R1, F2-R1, and F3-R1, respectively. These results indicate that the degradation of stiffness decreased with an increase in fire duration. The reason for the highest degradation of stiffness of slab F0-R1 was its highest initial stiffness in the first few cycles, whereas the initial stiffnesses of other slabs were significantly lower due to fire exposure.



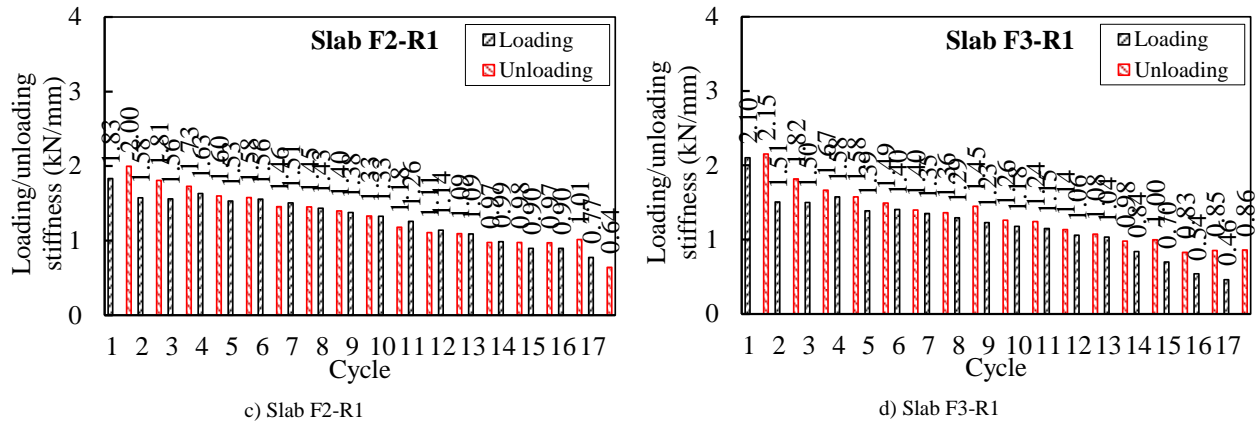


Figure 22. Loading and unloading stiffness

4. Theoretical Analysis

Figure 23-a shows the cross section of slabs, in which A_s , A_{gfrp} , and A_r are the cross-sectional areas of steel bars, GFRP bars, and resin, respectively, d and h are the effective depth and the height of slabs, respectively, a_0 is the concrete cover measured to the centre of tensile steel bars, d_{groove} and b_{groove} are the depth and width of grooves. The strain is assumed to be linearly distributed on the section (Figure 23-b). The stress on compressive concrete is shown in Figure 23-c, and its equivalent stress block is shown in Figure 23-d. Figure 23-e shows the tensile forces of steel (T_s) and NSM GFRP composite (T_{gfrpr}) and the compressive force (C), which are determined by Equations 2, 3, and 4, respectively. In these Equations, f_s , f_{gfrp} , and f_r are the stresses of steel bars, GFRP bars, and resin, respectively; a and $0.85f_c$ are the depth and the equivalent stress; b is the width of the slabs; and f'_c is the concrete strength.

$$T_s = f_s A_s \tag{2}$$

$$T_{gfrpr} = f_{gfrp} A_{gfrp} + A_r f_r \tag{3}$$

$$C = 0.85 f'_c a b \tag{4}$$

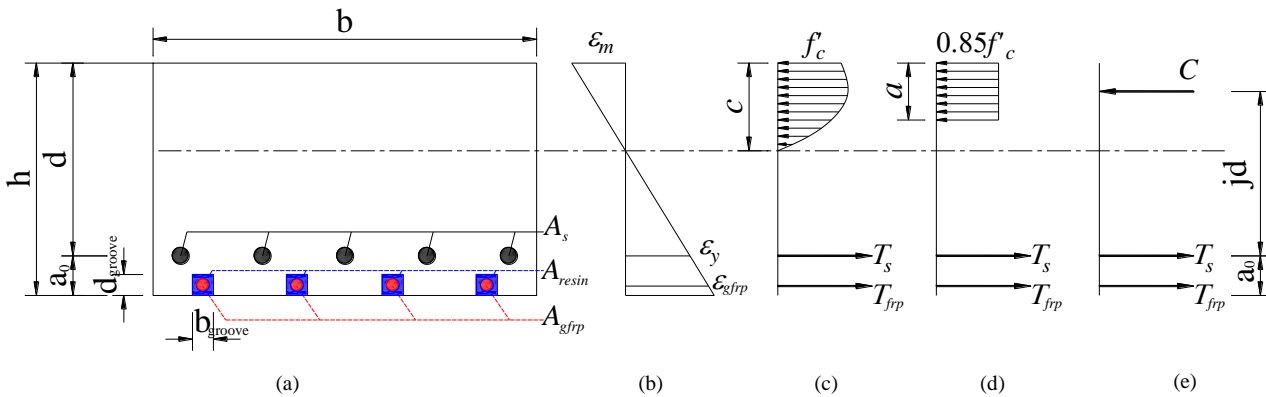


Figure 23. Theoretical analysis of slab section

The distances from the compression force C to the tension forces T_s and T_{gfrp} are shown by Equations 5 and 6, respectively, in which $a_{gfrp} = 0.5d_{groove}$ is the distance from the bottom surface to GFRP bars and d_{groove} is the depth of grooves.

$$jd = d - 0.5a \tag{5}$$

$$kh = h - 0.5a - a_{gfrp} \tag{6}$$

The bending moment, which is contributed by tensile steel and NSM GFRP composite forces with respect to the location of force C , is determined by Equation 7.

$$M = T_s jd + T_{gfrpr} kh \tag{7}$$

Equation 8 shows the equilibrium of forces. When steel yields, $T_s = T_y = A_s f_y$, and the moment is the yield moment. Equation 9 is obtained by substituting Equations 2 to 4 into Equation 8. Equation 10 is consequently derived to calculate the depth a .

$$C = T_s + T_{gfrpr} \tag{8}$$

$$0.85f'_c ab = A_s f_y + A_{gfrp} f_{gfrp} + A_r f_r \tag{9}$$

$$a = \frac{A_s f_y + A_{gfrp} f_{gfrp} + A_r f_r}{0.85f'_c b} \tag{10}$$

Equation 11 is gained by substituting Equations 5 and 6 into Equation 7. The yield bending moment is calculated by Equation 12, which is gained by substituting Equation 10 into Equation 11. In Equation 12, $f_{gfrp} = \varepsilon_{gfrp} E_{gfrp}$; $f_r = \varepsilon_r E_r = \varepsilon_{gfrp} E_r$; E_{gfrp} is the modulus strain of GFRP; and ε_{gfrp} is the strain of GFRP at the yielding state of steel. NSM GFRP bars are assumed to be positioned at the center of the grooves; thus, $\varepsilon_r = \varepsilon_{gfrp}$.

The depth c is determined by Equation 13, which is based on similar triangles related to the strain at the extreme concrete fibre ε_m and the yield strain of steel ε_y . This study adopted the commonly used value $\varepsilon_m = 0.003$. The strain of GFRP ε_{gfrp} is determined by Equation 14, which results from similar triangles related to the yield strain of steel ε_y . Equations 15 and 16 are derived from Equations 13 and 14, respectively. Equation 17 is gained by substituting Equation 15 into Equation 16, in which $s = 0.003/\varepsilon_y$.

$$M_y = A_s f_y (d - 0.5a) + (A_{gfrp} f_{gfrp} + A_r f_r) (h - 0.5a - a_{gfrp}) \tag{11}$$

$$M_y = A_s f_y \left(d - 0.59 \frac{A_s f_y + A_{gfrp} f_{gfrp} + A_r f_r}{f'_c b} \right) + (A_{gfrp} f_{gfrp} + A_r f_r) \left(h - 0.59 \frac{A_s f_y + A_{gfrp} f_{gfrp} + A_r f_r}{f'_c b} - a_{gfrp} \right) \tag{12}$$

$$\frac{c}{d-c} = \frac{0.003}{\varepsilon_y} \tag{13}$$

$$\frac{d-c}{h-c-a_{gfrp}} = \frac{\varepsilon_y}{\varepsilon_{gfrp}} \tag{14}$$

$$c = \frac{\frac{0.003}{\varepsilon_y} d}{1 + \frac{0.003}{\varepsilon_y}} \tag{15}$$

$$\varepsilon_{gfrp} = \varepsilon_y \frac{h-c-a_{gfrp}}{d-c} \tag{16}$$

$$\varepsilon_{gfrp} = \varepsilon_y \frac{h - \frac{sd}{1+s} - a_{gfrp}}{d - \frac{sd}{1+s}} = \varepsilon_y \frac{(h-a_{gfrp})(1+s) - sd}{d} \tag{17}$$

Yield moment of NSM GFRP retrofitted RC slabs is computed using Equation 12. This equation was developed based on the following assumptions: 1) the steel strength is fully recovered [29], 2) fire has no impact on the compressive concrete zone because this zone is on top of slabs (which was insulated), and 3) the reduction in steel-concrete bonding is negligible. Equation 12 can also be used for un-retrofitted RC slabs by simply deleting the terms related to the NSM GFRP composite. Column 2 of Table 4 presents the calculation results of yield moments. The analytical yield loads of the tested slabs were computed by $P_y = 4M_y/L$, where M_y is the analytical yield moment (column 2) and $L = 1.5$ m. The calculation results (column 3) are compared with the test results (column 4), and the comparison results are shown in column 5. The difference between the estimated yield moment and the experimental moment of the control slab is 9.6%. The difference between these two moments of the NSM GFRP retrofitted postfire slabs varies between 3.2% and 6.4%. These results demonstrate the accuracy of the theoretical equation of yield moment of NSM GFRP retrofitted postfire slabs; thus, this equation of yield moment can be used for practical application in practice.

Table 4. Yield load-carrying capacity

Slab	Analytical yield moment (kNm)	Yield load (kN)		Difference (%)
		Analysis	Test	
F0-R0	4.9756	13.3	12.1	9.6
F1-R0	6.4054	17.1	18.3	-6.4
F2-R0	6.4054	17.1	17.7	-3.5
F3-R0	6.4054	17.1	17.8	-3.7
F0-R1	6.4054	17.1	17.7	-3.2
F1-R1	6.4054	17.1	17.8	-3.9
F2-R1	6.4054	17.1	18	-5.1
F3-R1	6.4054	17.1	17.9	-4.5

5. Conclusions

The following conclusions are drawn:

- The control slab failed in flexure, with steel yielding and a main crack at the mid-span. NSM GFRP retrofitted postfire slabs failed by either crushing of compressive concrete or rupture of GFRP bars. NSM GFRP retrofitting substantially improved the behavior of postfire slabs. The tested slabs can be well characterized by bi-linear behavior.
- Despite the negative effects of fires, NSM GFRP retrofitting significantly improved the mechanical properties of postfire slabs. NSM GFRP retrofitting improved the yield and ultimate loads of postfire slabs by 47.2% and 116.4% on average, respectively. Fire duration is confirmed to be a main factor that significantly reduced the elastic stiffness of NSM GFRP retrofitted postfire slabs by 60.9% for 60 min of fire. The average plastic-to-elastic stiffness of NSM GFRP retrofitted postfire slabs was 0.132, which was 32 times that of the control slab.
- The cyclic loading effect caused substantial stiffness degradation of NSM GFRP retrofitted postfire slabs. The stiffness degradation increased with the increase in fire duration. The average stiffness degradations were 10.6% and 7.2% for un-retrofitted original and NSM GFRP retrofitted postfire slabs, respectively. However, the cyclic loading effect caused negligible strength degradation. The lower stiffness degradation of NSM GFRP retrofitted postfire slabs can be attributed to the lower initial stiffness of these slabs than that of NSM GFRP retrofitted original slabs due to the reduction in tensile and bond strengths of concrete. The combination of the increase in fire duration and the cyclic loading effect significantly decreased the ductility to moderate or low ductility.
- Theoretical analyses were carried out to estimate the yield moments of slabs without and with NSM GFRP retrofitting. The analytical yield moments are close to those obtained from experiments. With a negligible difference of less than 6.4%, the analytical equation demonstrated its accuracy in estimating the yield moment capacity of postfire RC slabs without and with NSM GFRP retrofitting.

6. Declarations

6.1. Data Availability Statement

The data presented in this study are available in the article.

6.2. Funding

The author received no financial support for the research, authorship, and/or publication of this article.

6.3. Acknowledgements

The author acknowledges Ho Chi Minh City University of Technology (HCMUT), VNU-HCM for supporting this study. The author thanks workers for their help on physical work with reasonable payment.

6.4. Conflicts of Interest

The author declares no conflict of interest.

7. References

- [1] Behnam, B. (2019). Fire Structural Response of the Plasco Building: A Preliminary Investigation Report. *International Journal of Civil Engineering*, 17(5), 563–580. doi:10.1007/s40999-018-0332-x.
- [2] Weerasinghe, P., Nguyen, K., Mendis, P., & Guerrieri, M. (2020). Large-scale experiment on the behavior of concrete flat slabs subjected to standard fire. *Journal of Building Engineering*, 30. doi:10.1016/j.jobbe.2020.101255.
- [3] Nguyen, V. N., & Cao, V. Van. (2023). Experimental and Analytical Study on Postfire Reinforced Concrete Beams Retrofitted with CFRP in Flexure and Shear. *Civil Engineering Journal (Iran)*, 9(7), 1610–1629. doi:10.28991/CEJ-2023-09-07-05.
- [4] da Costa, L. M., de Carvalho Pires, T. A., & Silva, J. J. R. (2023). Shear strengthening of fire-damaged reinforced concrete beams using NSM CFRP laminates. *Engineering Structures*, 287, 116175. doi:10.1016/j.engstruct.2023.116175.
- [5] El-Hacha, R., & Rizkalla, S. H. (2004). Near-surface-mounted fiber-reinforced polymer reinforcements for flexural strengthening of concrete structures. *ACI Structural Journal*, 101(5), 717–726. doi:10.14359/13394.
- [6] Bilotta, A., Ceroni, F., Nigro, E., & Pecce, M. (2015). Efficiency of CFRP NSM strips and EBR plates for flexural strengthening of RC beams and loading pattern influence. *Composite Structures*, 124, 163–175. doi:10.1016/j.compstruct.2014.12.046.
- [7] De Lorenzis, L., & Teng, J. G. (2007). Near-surface mounted FRP reinforcement: An emerging technique for strengthening structures. *Composites Part B: Engineering*, 38(2), 119–143. doi:10.1016/j.compositesb.2006.08.003.

- [8] Nguyen, V. N., & Van Cao, V. (2023). NSM GFRP Strengthening of Reinforced Concrete Beams after Exposure to Fire: Experiments and Theoretical Model. *Journal of Composites for Construction*, 27(1). doi:10.1061/jccof2.cceng-3933.
- [9] Kara, I. F., Ashour, A. F., & Koroğlu, M. A. (2016). Flexural performance of reinforced concrete beams strengthened with prestressed near-surface-mounted FRP reinforcements. *Composites Part B: Engineering*, 91, 371–383. doi:10.1016/j.compositesb.2016.01.023.
- [10] Nguyen, V. N., & Cao, V. Van. (2023). Performance of Postfire Reinforced Concrete Beams Retrofitted with External Bonded and Near-Surface Mounted CFRP: Experiments and Analyses. *Journal of Performance of Constructed Facilities*, 37(3), 04023016. doi:10.1061/jpcfev.cfeng-4297.
- [11] Yang, J., & Wang, L. (2018). Experimental research on flexural behaviors of damaged PRC beams strengthened with NSM CFRP strips. *Construction and Building Materials*, 190, 265–275. doi:10.1016/j.conbuildmat.2018.09.109.
- [12] Zhang, S. S., Yu, T., & Chen, G. M. (2017). Reinforced concrete beams strengthened in flexure with near-surface mounted (NSM) CFRP strips: Current status and research needs. *Composites Part B: Engineering*, 131, 30–42. doi:10.1016/j.compositesb.2017.07.072.
- [13] Gravina, R., Aydin, H., & Visintin, P. (2018). Review of near-surface mounted FRP plates in the strengthening of continuous flexural members and bond behavior. *Australian Journal of Civil Engineering*, 16(2), 158–165. doi:10.1080/14488353.2018.1537594.
- [14] Al-Saadi, N. T. K., Mohammed, A., Al-Mahaidi, R., & Sanjayan, J. (2019). A state-of-the-art review: Near-surface mounted FRP composites for reinforced concrete structures. *Construction and Building Materials*, 209, 748–769. doi:10.1016/j.conbuildmat.2019.03.121.
- [15] Sabbaghian, M., & Kheyroddin, A. (2020). Flexural strengthening of RC one-way slabs with high-performance fiber-reinforced cementitious composite laminates using steel and GFRP bar. *Engineering Structures*, 221. doi:10.1016/j.engstruct.2020.111106.
- [16] Silva, M. A. L., & Gamage, J. C. P. H. (2020). Combined effects of Carbon Fiber Reinforced Polymer flexural reinforcements and post installed shear dowels on the performance of flat slabs. *Composite Structures*, 236. doi:10.1016/j.compstruct.2019.111848.
- [17] Yazdani, S., Asadollahi, S., Shoaie, P., & Dehestani, M. (2021). Failure stages in post-tensioned reinforced self-consolidating concrete slab strengthened with CFRP layers. *Engineering Failure Analysis*, 122. doi:10.1016/j.engfailanal.2021.105219.
- [18] Kamonna, H. H., & Al-Sada, D. J. A. (2021). Strengthening of one-way reinforced concrete slabs using near surface mounted bars. *Materials Today: Proceedings*, 42, 1843–1853. doi:10.1016/j.matpr.2020.12.215.
- [19] Zheng, X., Wan, B., Huang, P., & Huang, J. (2019). Experimental study of hybrid strengthening technique using carbon fiber laminates and steel plates for reinforced concrete slabs. *Construction and Building Materials*, 210, 324–337. doi:10.1016/j.conbuildmat.2019.03.100.
- [20] Kankeri, P., Suriya Prakash, S., & Pachalla, S. K. S. (2018). Experimental and Numerical Studies on Efficiency of Hybrid Overlay and Near Surface Mounted FRP Strengthening of Pre-cracked Hollow Core Slabs. *Structures*, 15, 1–12. doi:10.1016/j.istruc.2018.05.003.
- [21] Kodur, V. K. R., & Bhatt, P. P. (2018). A numerical approach for modeling response of fiber reinforced polymer strengthened concrete slabs exposed to fire. *Composite Structures*, 187, 226–240. doi:10.1016/j.compstruct.2017.12.051.
- [22] Bilotta, A., Compagnone, A., Esposito, L., & Nigro, E. (2020). Structural behavior of FRP reinforced concrete slabs in fire. *Engineering Structures*, 221. doi:10.1016/j.engstruct.2020.111058.
- [23] Huang, Z. (2010). The behavior of reinforced concrete slabs in fire. *Fire Safety Journal*, 45(5), 271–282. doi:10.1016/j.firesaf.2010.05.001.
- [24] Lim, L., Buchanan, A., Moss, P., & Franssen, J. M. (2004). Numerical modelling of two-way reinforced concrete slabs in fire. *Engineering Structures*, 26(8), 1081–1091. doi:10.1016/j.engstruct.2004.03.009.
- [25] Huang, Z., Burgess, I. W., & Plank, R. J. (2003). Modeling Membrane Action of Concrete Slabs in Composite Buildings in Fire. II: Validations. *Journal of Structural Engineering*, 129(8), 1103–1112. doi:10.1061/(asce)0733-9445(2003)129:8(1103).
- [26] Huang, Z., Burgess, I. W., & Plank, R. J. (2003). Modeling Membrane Action of Concrete Slabs in Composite Buildings in Fire. I: Theoretical Development. *Journal of Structural Engineering*, 129(8), 1093–1102. doi:10.1061/(asce)0733-9445(2003)129:8(1093).
- [27] Huang, Z., Burgess, I. W., & Plank, R. J. (2000). Effective stiffness modelling of composite concrete slabs in fire. *Engineering Structures*, 22(9), 1133–1144. doi:10.1016/S0141-0296(99)00062-0.
- [28] Lim, L., Buchanan, A., Moss, P., & Franssen, J.-M. (2004). Computer Modeling of Restrained Reinforced Concrete Slabs in Fire Conditions. *Journal of Structural Engineering*, 130(12), 1964–1971. doi:10.1061/(asce)0733-9445(2004)130:12(1964).

- [29] Moss, P. J., Dhakal, R. P., Wang, G., & Buchanan, A. H. (2008). The fire behavior of multi-bay, two-way reinforced concrete slabs. *Engineering Structures*, 30(12), 3566–3573. doi:10.1016/j.engstruct.2008.05.028.
- [30] Yu, X., & Huang, Z. (2008). An embedded FE model for modelling reinforced concrete slabs in fire. *Engineering Structures*, 30(11), 3228–3238. doi:10.1016/j.engstruct.2008.05.004.
- [31] Wang, Y., Yuan, G., Huang, Z., Lyu, J., Li, Q., & Long, B. (2018). Modelling of reinforced concrete slabs in fire. *Fire Safety Journal*, 100, 171–185. doi:10.1016/j.firesaf.2018.08.005.
- [32] Azevedo, A. S., Firmo, J. P., Correia, J. R., Firouz, R. M., & Barros, J. A. O. (2023). Fire behavior of reinforced concrete slab strips strengthened with prestressed NSM-CFRP laminates. *Engineering Structures*, 297. doi:10.1016/j.engstruct.2023.116982.
- [33] Rosa, I. C., Santos, P., Firmo, J. P., & Correia, J. R. (2020). Fire behavior of concrete slab strips reinforced with sand-coated GFRP bars. *Composite Structures*, 244. doi:10.1016/j.compstruct.2020.112270.
- [34] Wang, Y., Dong, Y. L., Li, B., & Zhou, G. C. (2013). A fire test on continuous reinforced concrete slabs in a full-scale multi-story steel-framed building. *Fire Safety Journal*, 61, 232–242. doi:10.1016/j.firesaf.2013.08.005.
- [35] Wang, Y., Yuan, G., Huang, Z., Lyv, J., Li, Z. Q., & Wang, T. yan. (2016). Experimental study on the fire behavior of reinforced concrete slabs under combined uni-axial in-plane and out-of-plane loads. *Engineering Structures*, 128, 316–332. doi:10.1016/j.engstruct.2016.09.054.
- [36] Wang, Y., Jiang, Y., Huang, Z., Li, L., Huang, Y., Zhang, Y., Zhang, G., Zhang, X., & Duan, Y. (2021). Post-fire behavior of continuous reinforced concrete slabs under different fire conditions. *Engineering Structures*, 226. doi:10.1016/j.engstruct.2020.111342.
- [37] Gao, W. Y., Hu, K. X., Dai, J. G., Dong, K., Yu, K. Q., & Fang, L. J. (2018). Repair of fire-damaged RC slabs with basalt fabric-reinforced shotcrete. *Construction and Building Materials*, 185, 79–92. doi:10.1016/j.conbuildmat.2018.07.043.
- [38] Sui, Z. A., Dong, K., Jiang, J., Yang, S., & Hu, K. (2020). Flexural behavior of fire-damaged prefabricated RC Hollow slabs strengthened with CFRP versus TRM. *Materials*, 13(11), 2556. doi:10.3390/ma13112556.
- [39] TCVN 7570. (2006). Aggregates for concrete and mortar – Specifications. Vietnam Standard, Hanoi, Vietnam. (In Vietnamese).
- [40] ACI 318-19. (2019). Building code requirements for structural concrete. American Concrete Institute (ACI), Michigan, United States.
- [41] ACI 440.2R-17. (2017). Guide for the design and construction of externally bonded FRP systems for strengthening concrete structures. American Concrete Institute (ACI), Michigan, United States.
- [42] Singh, S. B., Reddy, A. L., & Khatri, C. P. (2014). Experimental and Parametric Investigation of Response of NSM CFRP-Strengthened RC Beams. *Journal of Composites for Construction*, 18(1), 04013021. doi:10.1061/(asce)cc.1943-5614.0000411.
- [43] Kalayci, A. S., Yalim, B., & Mirmiran, A. (2010). Construction tolerances and design parameters for NSM FRP reinforcement in concrete beams. *Construction and Building Materials*, 24(10), 1821–1829. doi:10.1016/j.conbuildmat.2010.04.022.
- [44] Soliman, S. M., El-Salakawy, E., & Benmokrane, B. (2010). Flexural behavior of concrete beams strengthened with near surface mounted fibre reinforced polymer bars. *Canadian Journal of Civil Engineering*, 37(10), 1371–1382. doi:10.1139/L10-077.
- [45] Sharaky, I. A., Selmy, S. A. I., El-Attar, M. M., & Sallam, H. E. M. (2020). The influence of interaction between NSM and internal reinforcements on the structural behavior of upgrading RC beams. *Composite Structures*, 234. doi:10.1016/j.compstruct.2019.111751.
- [46] ASCE/SEI 41-06. (2007). Seismic rehabilitation of existing buildings. American Society of Civil Engineers (ASCE), Reston, United States. doi:10.1061/9780784408841.